In silico investigation of the thermochemistry and photoactivity of pyruvic acid in an aqueous solution of NaCl

Rodolphe Pollet, Wutharath Chin

In silico investigation of the thermochemistry and photoactivity of pyruvic acid in an aqueous solution of NaCl

Rodolphe Pollet*,† and Wutharath Chin‡

†*Université Paris-Saclay, CEA, CNRS, NIMBE, 91191, Gif-sur-Yvette, France.*

‡*Université Paris-Saclay, CNRS, Institut des Sciences Moléculaires d'Orsay, 91405, Orsay, France*

E-mail: rodolphe.pollet@cea.fr

Phone: +33 (1)690 83713

Abstract

The photochemistry of oxo-carboxylic acids contributes significantly to the complex chemistry occurring in the atmosphere. In this regard, pyruvic acid undergoes photoreactions that lead to many diverse products. The presence of sodium cation near pyruvic acid in an aqueous solution, or its conjugate base in non-acidic conditions, influences the hydration equilibrium and the photosensitivity to UV-visible light of the oxocarboxylic acid. We performed an ab initio metadynamics simulation which serves two purposes: first, it unveils the mechanisms of the reversible hydration reaction between the keto and the diol forms, with a free-energy difference of only 2 kJ/mol at 300 K, which shows the influence of sodium on the keto/diol ratio; second, it provides solvent-shared ion pairing (SSIP) and contact ion pairing (CIP) structures, including Na^+ coordinated to carbonyl, for the calculations of the electronic transition energies to an antibonding $\pi^\star$ orbital, which sheds light on the photoactivity of these two forms in the actinic region.

Introduction

The chemical reactivity of volatile organic compounds is intrinsically of multiphasic nature (gas, particle, liquid).[1] It is most complex for it involves phase-dependent reactions. Among them, some organics play a significant role in the formation of secondary organic aerosols.[2–4] Marine aerosols, fog, and cloud droplets are the sink of numerous and complex photochemical reactions involving water. Many studies have been devoted to processes in neat water, while fewer have focused on aqueous solutions with electrolytes. Fog and cloud droplets are characterized by dilute electrolyte conditions[5] but higher ionic strength can be found in aerosol deliquescent particles[6] or in marine aerosols.[7] Ions can impact the properties of aqueously solvated compounds in different ways, in particular by acting on their photoactivity. The ion content may indeed greatly affect the optical absorption and hence the fate of atmospheric compounds upon solar irradiation. It was reported that relatively high ion concentrations

as found in marine conditions[7] could induce a bathochromic effect on the absorption of anionic chromophores.[8,9] The spectral shift can be significant enough to photo-sensitize a photo-inactive compound, i.e., that initially does not absorb in the actinic region.

Pyruvic acid (PA), an oxidation product of isoprene, is the smallest and the most prevalent 2-oxo carboxylic acid in the atmosphere.[10–13] Its photochemical behavior has been widely investigated in water.[13–18] PA is assumed to contribute to the formation of secondary organic aerosols since its direct and indirect photolysis yield oxidized products and oligomers of higher mass.[19–25] Aqueous-phase pyruvic acid exists as four different species. The keto and the gem-diol forms are in equilibrium and both can be protonated or deprotonated according to the pH conditions (pK_a = 1.7-2.2).[26,27] The keto species contribute to the photoactivity of PA in the atmospherically relevant region,[13,15,16,28–30] while the diol absorbs out of the actinic window below 290 nm. The photochemistry of the acidic form has received a lot of attention but in water unless at low pH conditions,[14,15,26] PA is mainly present as the anionic pyruvate species[15,16,31–35] It was found that the optical properties were affected by the presence of salts by inducing for instance a bathochromic effect that varies upon the nature of the ion and the pH conditions.[8,16,36] Are these changes dictated by direct interactions between the ion and the anionic chromophore or is it due to the disruption of the hydrogen bonding network in water.[9] A better comprehension of how electrolytes such as Na^+ influence the photoactivity of pyruvate can shed light on the perturbation induced by ions close to anionic chromophores. The ion content also significantly impacts the stabilization of the ketone and diol species and hence the keto-diol equilibrium.[16]

Theoretical investigations with an atomic scale resolution can reveal such organic molecules' structural and thermodynamical properties in salted water. As to PA, most of these studies have focused on geometries and energies of the ketone or diol form in the vacuum, continuum solvent, or surrounded by a few explicit water molecules.[15,16,33,37–39] However we have previously demonstrated that solvent effects need to be fully taken into account for an accurate prediction of these properties,[32] and this should still hold true in the presence of

electrolytes. In explicit aqueous solution at finite temperature, chemical reactions such as the diol formation can be accurately described by ab initio molecular dynamics simulations (AIMD) coupled to accelerated sampling techniques. On an unbiased simulation timescale, such a reactive event would be too rare preventing the reconstruction of the corresponding free-energy landscape including free-energy minima and barriers.

In the present work, we combine the Car-Parrinello (CP) and the metadynamics (MTD) methods to describe the reversible hydration of the conjugate base of PA in salted water and to select the relevant configurations of ketone and diol hydrated complexes with Na^+ for excited-state calculations. Our simulation of the aqueous solution of NaCl has been designed with an ionic strength of approximately 0.5 M (see Computational Details), which is close to typical seawater, therefore this work provides detailed reaction mechanisms for the hydration and the dehydration of PA which should be relevant for nascent sea spray aerosols.[40] In addition, the UV-visible spectroscopic data gauge the effect of Na^+ on its photoactivity.

Results and Discussion

Pyruvate-sodium pair in water from the unbiased simulation

The ab initio simulation without any bias potential provides a description of the competing interactions that involve pyruvate, Na^+, and surrounding water molecules. Under these conditions, there is one conformational family, where Na^+ strongly interacts with one carboxylate oxygen (O_1 atom) only at an average distance of 2.29 (0.15) Å (Figure 1). It is identified as a contact ion pair (CIP) in a monodentate mode. This configuration significantly differs from the bidentate geometry between the carboxylate group of pyruvate and Ca^{2+} reported by Luo *et al.*[16] This difference may have several origins. In spite of its similar size to Na^+, the increased charge of Ca^{2+} results in higher polarizability, which may favor a bidentate structure. In addition, in the study by Luo *et al.*, the optimization at 0 K and

the smaller size of the system, i.e., pyruvate surrounded by only six water molecules, may not fully describe the entropic and solvent effects. During the last 20 ps, Na^+ gets closer to the O_3 carbonyl oxygen with an average distance of 4.44 (0.30) Å (Figure 2).

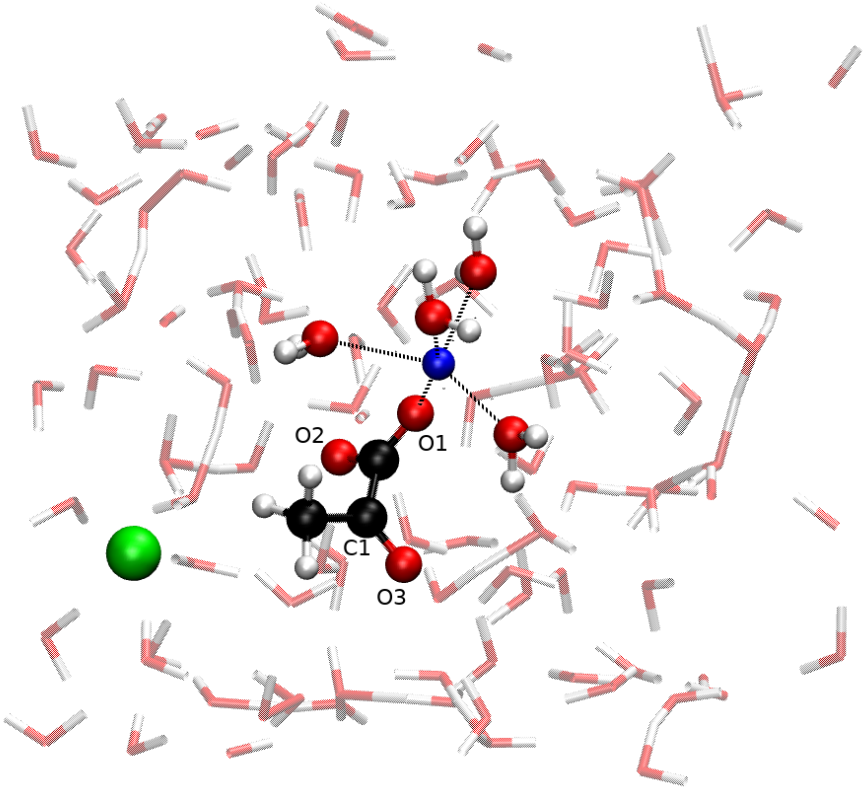

Figure 1: Representative configuration showing four water molecules and one carboxylate oxygen of keto pyruvate coordinated to Na^+ (blue color), other solvent molecules (transparent), and Cl^- (green).

We now examine each entity of the CIP, starting with the cation. The coordination structure of Na^+ is composed of the O_1 carboxylate oxygen and four water molecules in a distorted trigonal bipyramidal geometry (Figure 1 and Figure S2 in Supplementary Information). Two of these water molecules exhibit a few exchanges between the first and second solvation shells. The geometry of the pyruvate anion is perpendicular with a $O_3C_1CO_1$ dihedral angle of -94 (±18) degrees. It is very close to the value of -92 degrees observed for pyruvate in neat water[32] and it matches very well the perpendicular structures reported in the literature.[33,38] The O_3 carbonyl oxygen mostly accepts two hydrogen bonds from the

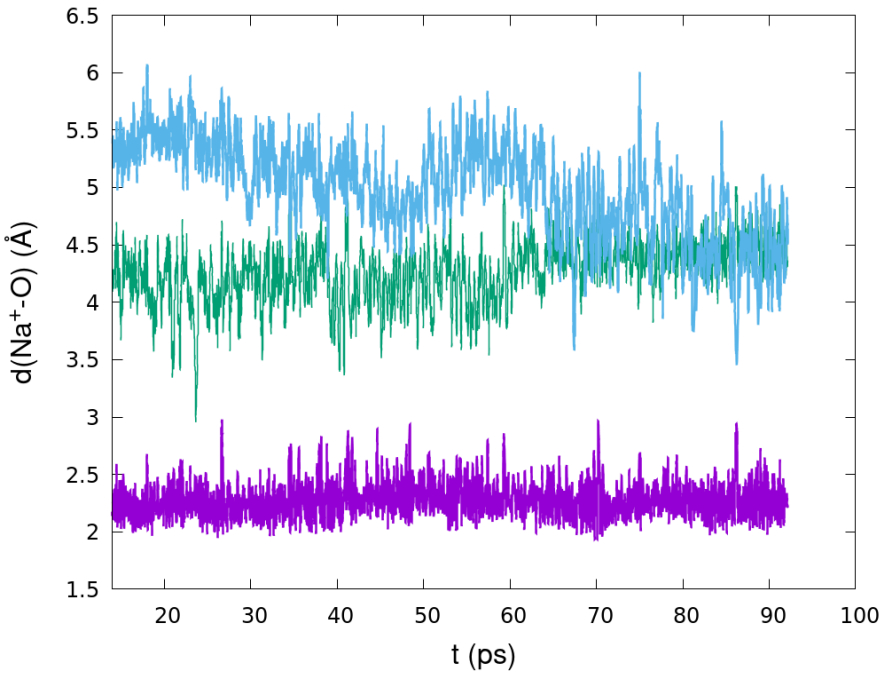

Figure 2: Distances (in Å) between Na^+ and (i) the carboxylate oxygen atoms in a CIP geometry (O_1 in purple and O_2 in green); (ii) the carbonyl oxygen atom O_3 (in blue) along the CP trajectory.

surrounding water molecules, except for the last 17 ps, where only one hydrogen bond is present. This change in the hydrogen bonding is presumably linked to the approach of the cation closer to O_3 as shown by the shorter distance between Na^+ and O_3 in Figure 2. This proximity introduces competition between water interacting with O_3 through hydrogen bonding or between water interacting with Na^+. The latter appears more favorable. We showed previously that the hydration reaction of the keto form involved the carbonyl group.[32] Therefore, one can expect that the keto-diol equilibrium is impeded compared to neat water conditions since the carbonyl is now less exposed to water. It will be discussed in the next section presenting the metadynamics results.

Reversible hydration of pyruvate

The hydration of pyruvate has been reversibly observed along the accelerated metadynamics trajectory. Here we present the relative free-energy minima and barriers, and we discuss

the structures that represent each species. Figure 3 shows the reconstructed free-energy landscape along the two collective variables (CV) which were designed to promote the hydration reaction, namely the coordination number (CN) of O_3 to all water hydrogen atoms ($O_3 \cdots H_W$) and the CN of C_1 to all water oxygen atoms ($C_1 \cdots O_W$) (see Computational Details). Two main free-energy basins are identified: The keto and the gem-diol forms of pyruvate. Their corresponding minima are located at coordinates (0.32, 0.16) and (1.16, 0.88), respectively. The former, with low coordination numbers, indeed corresponds to the unhydrated species, whereas the latter, with large coordination numbers, corresponds to a geminal diol with two hydroxyl groups. The transition state is located at intermediate values at approximately (0.7, 0.6). In the presence of sodium, the diol is favored by approximately 2 kJ/mol with respect to the keto. It is much lower than the value found in neat water where the diol was more stable by 16 kJ/mol,[32] showing that the hydration is more exergonic in water. Consequently, the free-energy barriers which we estimate at 71 kJ/mol for hydration and at 73 kJ/mol for dehydration are comparable. The energetic difference between the barriers calculated in our previous study in water was much higher at 68 and 84 kJ/mol, respectively.[32] It means that the dehydration process requires less energy in salted conditions, thereby favoring the keto species at the expense of the diol species. It is in good agreement with the lower diol/keto ratio measured in salted water (with Na^+ and Ca^{2+} cations).[16]

We identified several pathways for hydration and dehydration reactions. From the keto form to the diol, the first path proceeds in four steps (see Figure 4): (a) Na^+ is coordinated to the O_3 carbonyl (average distance of 2.18 Å), the geometry changes simultaneously from perpendicular to planar; (b) there is a concerted attack of two water molecules onto O_3 and C_1; (c) the first hydroxyl is formed on C_1; (d) the second hydroxyl is formed on O_3 yielding the diol species. This mechanism is similar to what was observed in neat water, with the first hydroxyl formed on the carbonyl carbon atom.[32] A second path starts from a monodentate CIP configuration, with Na^+ bound to O_1 carboxylate (average distance of 2.31 Å) and closer to C_1 carbonyl, (see Figure 5). The following steps lead to the diol: (a) a water molecule

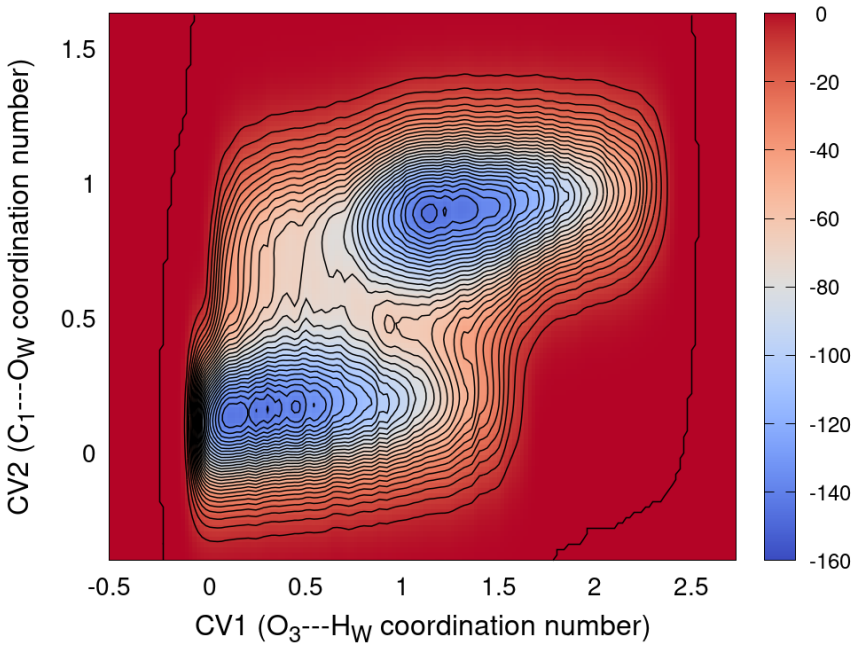

Figure 3: Free-energy landscape (in kJ/mol). CV1 ($O_3 \cdots H_W$ coordination number) as the x-axis and CV2 ($C_1 \cdots O_W$ coordination number) as the y-axis.

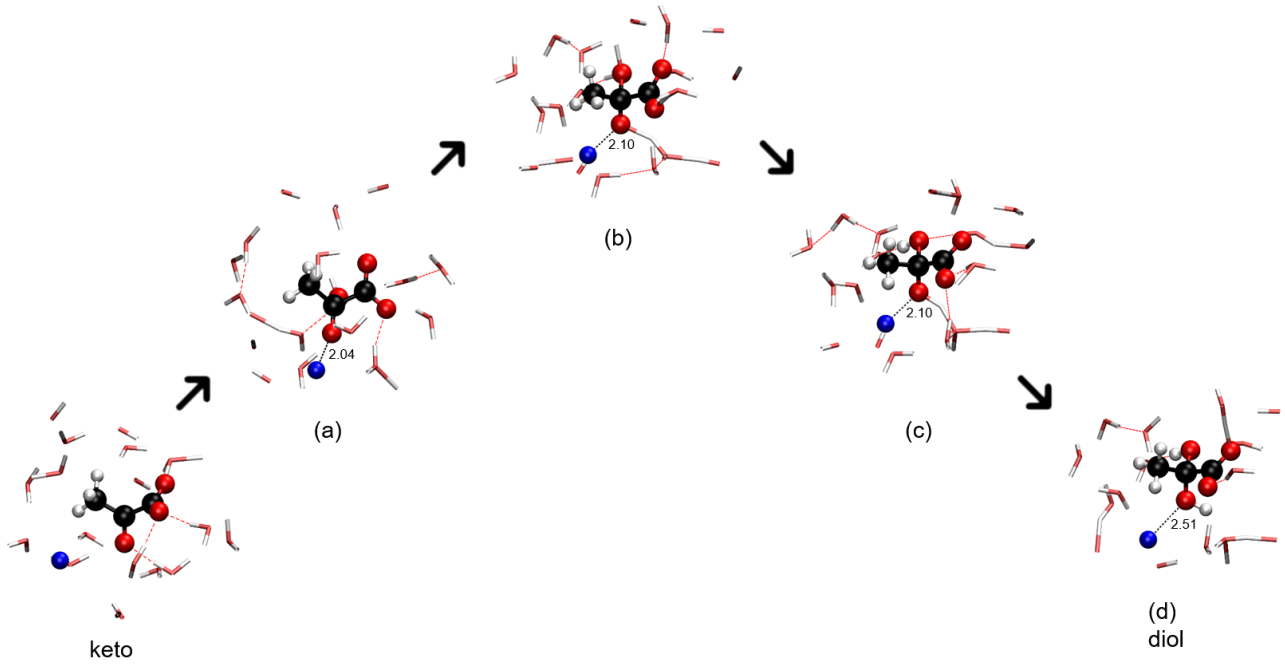

Figure 4: First hydration pathway (from keto to diol pyruvate) observed during the metadynamics: (a) coordination of Na^+ to the O_3 carbonyl; (b) concerted attack of two water molecules; (c) formation of the first hydroxyl on the C_1 site; (d) formation of the second hydroxyl on the O_3 site. See text for details. Most of the solvent molecules are not shown.

shares one hydrogen with O_3 through hydrogen-bonding; (b) the first hydroxyl is formed on the O_3 site simultaneously with the formation of a chain of hydrogen-bonded water molecules; (c) the second hydroxyl is formed on the C_1 site after a cascade of proton transfers giving the diol. Although the first hydroxyl is formed here on O_3 carbonyl, the second hydroxyl appears after only a few MD steps, which is akin to a concerted reaction. Both hydration

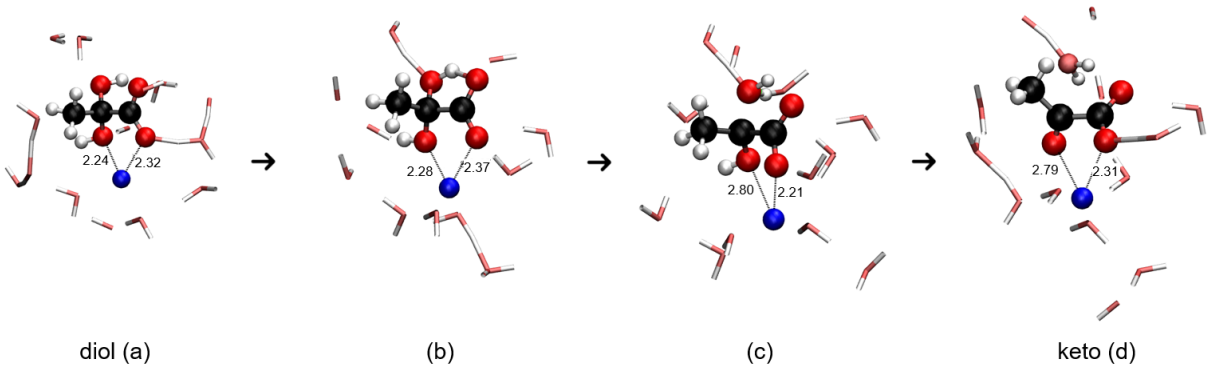

Figure 5: Second hydration pathway (from keto to diol pyruvate) observed during metadynamics: (a) hydrogen shared between water and O_3; (b) formation of the first hydroxyl on O_3; (c) formation of the second hydroxyl on C_1. See text for details. Most of the solvent molecules are not shown.

paths involve direct interactions with the carbonyl group but the precise mechanisms are distinct. In the first hydration path, O_3 is less available for water attack because of the close contact with Na^+ (2.04 Å in Figure 4a). This interaction polarizes the carbonyl bond rendering the C_1 carbon atom more electrophilic and hence more prone to water attack, explaining the formation of the first hydroxyl on this site. After this step, Na^+ moves away from pyruvate (2.10 then 2.51 Å), leaving room for the hydration on the O_3 site by water. In the second path, Na^+ is close to the carboxylate oxygen (2.31 Å in Figure 5a). Therefore the approach of water towards O_3 carbonyl is not hindered so that the first hydroxyl is formed on the O_3 site. The formation of a chain of hydrogen-bonded water molecules is enabled by the electrostatic interaction between Na^+ and COO^-. This interaction is absent in neat water, preventing the appearance of such bridged water molecules.[32]

For the dehydration reaction (see Figure 6), the first path proceeds as follows: (a) Na^+ is

coordinated to O_3, which weakens the O_3-H hydroxyl bond; (b) a five-membered ring with a hydrogen atom bridging O_3 to the carboxylate oxygen is formed; (c) it is followed by the hydrogen-transfer to the carboxylate oxygen; (d) the carboxylic group then rotates towards a perpendicular geometry; (e) allowing for the formation of a hydrogen bridge between the remaining hydroxyl oxygen and the carboxylic hydrogen; (f) proton transfer to the hydroxyl group takes place giving a free water molecule and the keto species. An alternative

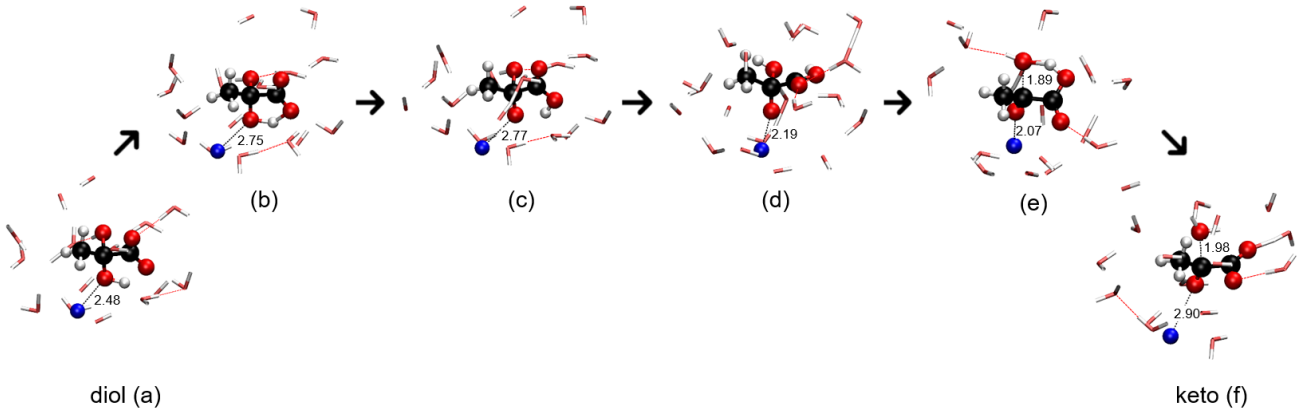

Figure 6: First dehydration pathway (from diol to keto pyruvate) observed during the metadynamics: (a) coordination of Na^+ to O_3; (b) formation of a five-membered ring; (c) proton transfer; (d) rotation of the carboxylic group; (e) formation of a hydrogen bridge; (f) proton transfer giving a free water molecule and the keto species. See text for details. Most of the solvent molecules are not shown.

dehydration path is also observed at the end of the metadynamics simulation (see Figure 7). The reaction also implies a five-membered ring but on the opposite side of Na^+: (a) Na^+ is coordinated to the carboxylate and one hydroxyl (at 2.34 and 2.42 Å, respectively) in a CIP bidentate geometry; (b) a five-membered ring is formed between the "free carboxylate" and the hydroxyl group at the opposite of Na^+; (c) the O-H detaches from the pyruvate giving a free water molecule; (d) the hydrogen from the other hydroxyl group dissociates to form the keto. The coordination of Na^+ therefore opens a novel "H-bridge" pathway. By weakening the hydroxyl bond, Na^+ triggers the dehydration reaction by allowing the formation of an intramolecular hydrogen bond, which favors a hydrogen transfer. It is a likely explanation for the lower free-energy barrier for the dehydration process (73 kJ/mol instead of 84 kJ/mol

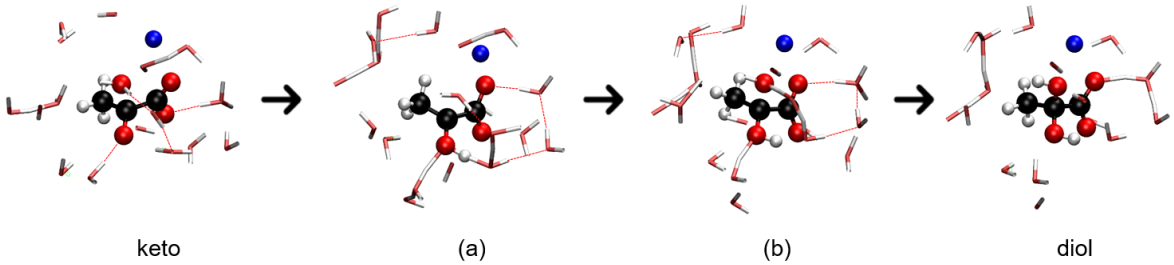

Figure 7: Second dehydration pathway observed at the end of the metadynamics: (a) bidentate coordination of Na^+ to OH and carboxylate; (b) formation of a five-membered ring on the opposite side; (c) detachment of O_3H to form a free water molecule; (d) dissociation of the other hydroxyl group (keto species). See text for details. Most of the solvent molecules are not shown.

in water) and hence for the reduced diol/keto ratio compared to neat water.

We present the separate structural analyses for the keto and diol forms and for the transition state region.To this aim, three families of configurations were extracted from the MTD trajectory based on the values of the two collective variables, according to some well-chosen boundaries. They respectively include 9893, 13925, and 1292 configurations. We observe that the transition state exhibits a protonated carboxylic group, whereas only the pyruvate anion is present in the keto and diol basins (see Figure S3 in Supplementary Information). In the case of the diol, the formation of the anionic species solely is certainly caused by the presence of the Na^+ cation, since a mixture of protonated and deprotonated diol forms was observed in neat water.[32] We now examine the interaction between the sodium cation and the pyruvate anion more closely. by discussing the $Na^+ \cdots O_3$ distance, d_{NaO_3}. Nearly 50% of the configurations at the bottom of the keto basin have the d_{NaO_3} distance fluctuating around 2.4 (0.3) Å, indicating that Na^+ is strongly coordinated to the carbonyl but has no contact with the carboxylate group. Such an interaction has been evidenced in several works although it is chemically not intuitive and seems non-standard. The X-ray crystal structure of sodium pyruvate reported a structure with a pseudo-five-membered ring where Na^+ connects with the carbonyl oxygen and one carboxylate oxygen.[41] More than 40% of the configurations show Na^+ lying further from O_3 carbonyl and coordinated to one carboxylate

oxygen in a monodentate CIP configuration (respective average distance of 4.5 (0.4) Å and 2.3 (0.1) Å). We do not observe any symmetrical bidentate CIP configuration between Na^+ and COO^-. It underlines that a simple intuition based on electrostatics only is not valid in salted water conditions. Less than 10 % of the configurations exhibit a solvent-shared ion pairing (SSIP) structure, with Na^+ in a fully solvated environment by water molecules (at more than 4 Å from pyruvate). On the pyruvate side, the interaction between Na^+ and O_3 directly impacts the structure of the anion. We indeed observe a strong correlation (i.e., Pearson coefficient of -0.7) between d_{NaO_3} and the torsion of pyruvate, with average OCCO dihedral angles of -56° (22°) and -105° (26°) for short and long d_{NaO_3} distances, respectively. In other words, the pyruvate keto tends to deviate from the perpendicular geometry[32,33,38] whenever Na^+ is coordinated to the O_3 carbonyl oxygen. This structural change is observed in the beginning of the first hydration path described above. Near the bottom of the diol basin, in contrast with keto, the SSIP structure is predominant (65% of the configurations) with Na^+ fully solvated by water and showing no coordination to pyruvate. It shows that overall the interaction between sodium and the anion is weaker for the diol. Other common configurations display a direct interaction between Na^+ and pyruvate. Almost 20% show a bidentate CIP structure where Na^+ is coordinated to the carboxylate and to one hydroxyl group. They present a five-membered ring structure formed by Na, O_1, C_2, C_1, and OH. Less than 15% are in a Na^+–hydroxyl monodentate mode. As to the transition state region, one common feature of all configurations is the presence of an oxygen atom (from a water molecule or a hydroxide ion) at 1.82 (± 0.06) Å from C_1, as already observed for glyoxylic and pyruvic acids in neat water although this distance was slightly larger.[32] For dehydration, Figure 6-b is representative of the transition state, with a five-membered ring structure formed by a hydrogen bridge and therefore a planar geometry.

To summarize, the metadynamics provides a more detailed picture of the structural arrangements than the unbiased CP simulation. It reveals crucial details on the different coordination modes of Na^+ to keto pyruvate, either involving the carboxylate or the carbonyl

groups. It also points out that solvent shared structures are favored for the cation-diol pair. Sodium is coordinated to pyruvate in all the identified hydration and dehydration processes. Importantly, Na^+ could act as a catalyst for the dehydration reaction since its coordination to pyruvate can trigger the formation of "H-bridge" structures leading to the keto form. Its impact on the photoactivity of pyruvate is examined in the next section.

Excitation of the keto and diol forms of pyruvate

The calculations of the vertical excited states for the keto and the diol species are presented in this section. All results are summarized in Table 1.

Table 1: Vertical excited state energies and oscillator strengths calculated with the ADC(2)/def2-TZVPP method for six configurations extracted from the the keto ($K_{i=1,3}$) and diol ($D_{i=1,3}$) free-energy basins. Na^+ is coordinated to carboxylate in K1 (CIP structure), to the O_3 carbonyl in K2 and in a SSIP geometry in K3. Na^+ is coordinated to a hydroxyl oxygen in D1, far from the pyruvate molecule in D2, or part of a five-membered ring structure in D3.

	S_1			S_2		
	E (eV)	E(nm)	f $\times 10^{-3}$	E (eV)	E(nm)	f $\times 10^{-3}$
K1	3.93	316	0.2	4.94	251	26.9
K2	3.45	359	1.4	4.07	304	24.4
K3	3.69	336	0.8	5.20	238	1.4
D1	3.74	331	0.7	4.35	285	3.2
D2	4.17	297	0.7	4.77	260	0.6
D3	4.87	255	0.2	5.17	240	1.3

The configurations in the keto basin have been described in the previous section. Briefly, K1 is representative of the monodentate Na^+-carboxylate (CIP) structures, K2 of the Na^+-carbonyl structures, and K3 of the SSIP configurations where Na^+ is screened by the solvent and is not coordinated to pyruvate. The geometries are displayed in Figure 8. For the excited states calculations, we keep only the closest water molecules (ten, nine, and nine, respectively). The S_1 states of K1, K2, and K3 configurations lie in the actinic region at 316, 359, and 336 nm, respectively. They show a very weak oscillator strength. For K1 and K3, only the $S_0 \rightarrow S_1$ transition is relevant to atmospheric purposes so excitations to

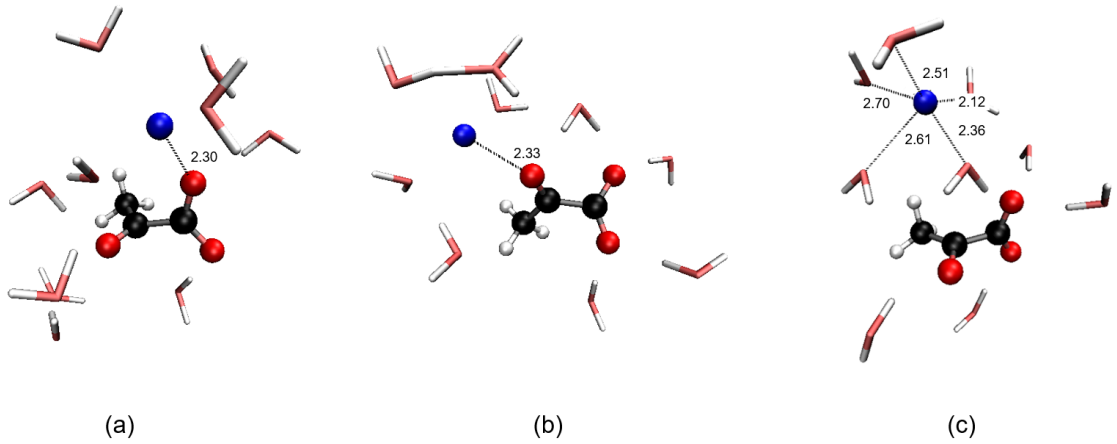

Figure 8: Representative configurations in the keto anion basin. Na^+ is coordinated to carboxylate in K1 (CIP structure), to the O_3 carbonyl in K2 and in a SSIP geometry in K3.

higher lying-states are not discussed further. The virtual natural transition orbitals (NTOs) of the S_1 states have a strong π^* character, and their associated occupied NTOs include the p-type lone pair (n) of the carbonyl oxygen (see Figures S4 to S6 in Supplementary Information). The S_1 state of K1 at 316 nm compares well with results reported in the literature. The absorption spectrum of bare pyruvate averaged over 500 structures, calculated at the SCS-ADC(2)/cc-pVTZ level by Clarke et al[33] is found to peak at 318 nm. The work of Cao et al. reports calculated absorption in the same domain for pyruvate and its micro-solvated complexes with up to five water molecules.[38] Our value also matches well the experimental absorption spectrum (maximum near 318 nm, see Figure S7 in Supplementary Information).[16] We note however differences with the calculations of Shemesh et al.[15] that predict a red-shifted absorption at 331-349 nm region. It is probably due to unconverged calculations yielding more planar geometries for pyruvate instead of perpendicular. In fact we also observe non perpendicular geometries in our simulation, represented by the K2 configuration where Na^+ is coordinated to the carbonyl group (average d_{NaO_3} = 2.38 Å and OCCO dihedral angle of -56°). We postulate that the close contact of the cation with the carbonyl chromophore dictates the more planar geometries of the K2-like configurations. The direct interaction of Na^+ with the main UV chromophore has a very strong impact (see

the NTO analysis in Supplementary Information). First, it induces a large 43 nm red-shift of the S_1 state compared with K1 (53 nm for S_2). Second, the oscillator strength of the $S_0 \rightarrow S_1$ transition of K2 is larger by one order of magnitude than its counterpart for K1 and K3. Moreover, the $S_0 \rightarrow S_2$ transition lies also in the actinic region at 304 nm and bears a very high oscillator strength. Hence not only K1-like configurations are relevant for the photochemistry of pyruvate but K2-like structures should also be taken into account since they may represent a large fraction of pyruvate in salted water. Experimentally, the red shift measured at elevated salt concentrations[8] (maximum absorption near 330 nm) could be rationalized by a larger contribution due to K2, where the cation directly interacts with the carbonyl chromophore.

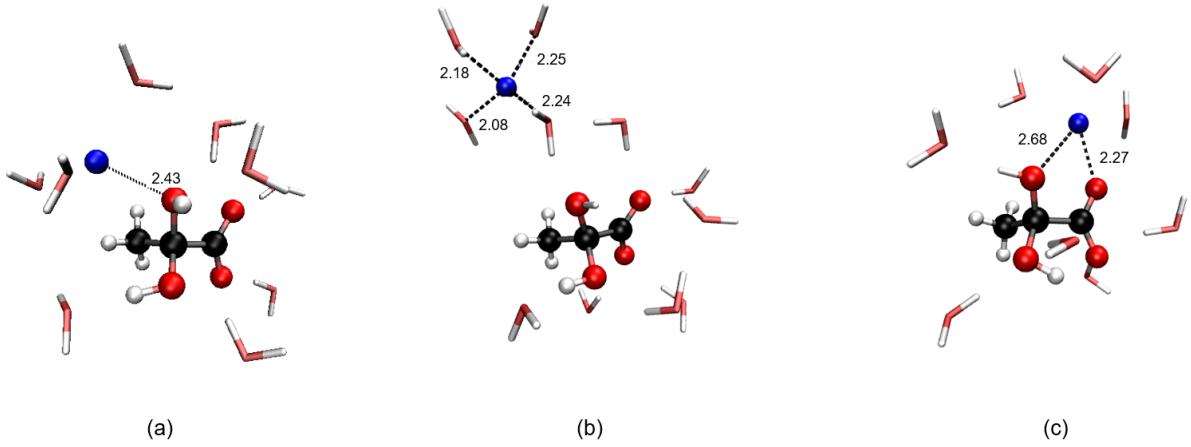

Figure 9: Representative configurations in the diol anion basin: a) D1, b) D2 (SSIP), c) D3 (CIP).

For comparison, we also calculated the vertical excitation energies of three representative configurations in the diol basin labeled D1, D2, and D3, mentioned previously in the Reversible hydration of pyruvate section. They respectively include 12, 9, and 8 water molecules (Figure 9). In the D1 configuration, Na^+ is in contact with one hydroxyl oxygen at a distance of 2.43 Å and is surrounded by three water molecules within a 2.60 Å distance. D1 shows no interaction between Na^+ and the carboxylate. In the D2 (SSIP) configuration, the Na^+ cation is far from the hydroxyl groups (at 4.64 Å from the closest one) and is fully solvated

by four water molecules. D3 configuration is a bidentate CIP geometry with Na^+ interacting with the carboxylate and one hydroxyl group (respectively at 2.27 and 2.68 Å). Similarly to keto, we have considered excitations to the S_1, S_2 states of the diols. The energies are given in Table 1. Interestingly, our whole set of computed energies is significantly lower than the values reported in the literature. To our knowledge, only two theoretical studies in the gas phase mention the electronic properties of the diol and its monohydrated complex with transitions lying above 5.6 eV.[15,39] The addition of water seems to induce a small down-shift in the transition of the neutral diol, and a slight up-shift in the case of the anion diol. It is unlikely that the difference between our values and literature only stems from the higher level of theory used in our approach or from the larger number of water molecules in our system. The discrepancy with the neutral diol can be understood in terms of the protonated state of the diol, i.e. deprotonated in the present work and neutral in Ref. 15,39. As to the anion diol, the higher excitation energy may result from the symmetrical structure considered in the work of Shemesh et al.[15] Our simulations in explicit water conditions - with or without electrolytes - exhibit no such symmetrical geometries which we think are not realistic in water. In aqueous solutions with electrolytes, PA exhibits experimental red-shifts of 2-13 nm depending on the nature and the concentration of the electrolytes.[8,16] It is much weaker than those found by our calculations on the diol, confirming that the diol is a minor species. However, the diol form may become a photosensitizer when it is predominant as in the case of acetic acid, glyoxylic acid,[42] glyoxal,[43] methylglyoxal,[44] etc.

Summary and conclusion

The ab initio metadynamics simulation in salted aqueous solution combined with excited states calculations has revealed that the sodium cation can interact with different parts of the pyruvate molecule, including the carbonyl group, thus impacting both its hydration equilibrium and its electronic absorption spectrum. A stringent consequence is that the

diol-to-keto ratio is reduced in comparison with neat water. Some dehydration pathways directly involving sodium have been observed and are a likely explanation for the decreased stabilization of the diol form in salted water conditions. New photochemical pathways with a direct interaction between sodium and the carbonyl chromophore could be explored for the keto species. Although it is clear that the monodentate contact ion pairs between Na^+ and the carboxylate are the favored geometries and are mainly responsible for the absorption spectrum of pyruvate, the stabilization of 'new' complexes such as sodium-carbonyl or sodium-diol can induce a significant bathochromic effect and therefore make them act as new photosensitizers. We assume that the entropic effects of water and the solvation of Na^+ probably prevent the stabilization of the bidentate configurations. Further investigations including the Ca^{2+} cation, which is generally assumed to bind to the carboxylate group in a bidentate mode, could reveal if similar influences on thermochemistry and photoactivity take place due to the cation mobility around the acid. More generally, the ionic strength has a crucial influence on the physical chemistry properties of oxo-carboxylic acids, and organic acids, and should be taken into account since compounds that do not present photochemistry in the actinic region may become photoactive in the presence of ions. This may have a strong effect on the formation of secondary organic aerosols.

Given the direct interaction of Na^+ with pyruvate, the present work also suggests that an improved free-energy landscape would be obtained by an extended metadynamics simulation incorporating additional collective variables as functions of the sodium cartesian coordinates. This would help disentangle the most stable configurations in each free-energy basin and estimate the free-energy barriers more accurately. Such time-consuming simulations could rely on methods such as the bias-exchange variant.[45]

Computational details

Ab initio molecular dynamics

The Car-Parrinello (CP) method[46,47] coupled to the metadynamics technique[45,48–52] was used within the CPMD code[53] to reconstruct the free-energy landscape of the hydration-dehydration reaction of pyruvate in an aqueous solution with NaCl. The computational details were given in our previous work[32] and we only briefly describe the present simulation (see also the monitoring of the fictitious kinetic energy in Figure S1). The system consists of a cubic supercell of 15 Å including PA, 108 water molecules, and one NaCl with a molarity and ionic strength of 0.49 M (as estimated from the volume of the box). Compared to Ref. 32, there is an additional NaCl electrolyte, and the size of the system is larger, which provides a better description of the aqueous solution. For Na^+, we use an ultrasoft pseudopotential[54] whose correctness has been proven on a system containing sodium oxide, where the $2s2p$ semicore electrons are excluded from the valence space.[55] In the initial configuration, this cation is coordinated to the two oxygen atoms of the carboxylate group O_1 and O_2. However, during the equilibration process, the configuration evolves towards a structure where Na^+ is solvated by more water molecules and is bound to O_1 carboxylate in a monodentate mode (Figure 1).

The whole simulation included a preliminary, unbiased, CP simulation of 91 ps, including an equilibration period of 13 ps, at a controlled temperature of 300 K, followed by an *ab initio* MTD simulation (in its extended Lagrangian version). Both forward and backward transitions of the reversible hydration reaction were explored in the same run with a unique set of collective variables (CVs), which requires several barrier recrossings. This strategy has been chosen instead of running separate runs for the forward and backward transitions with possibly distinct sets of CVs because it is more accurate although more time-consuming. We took the same two CVs and their associated parameters as those used in our previous study for the MTD calculations.[32] They were specifically designed to accelerate the formation of

the hydroxyl groups of the geminal diol form. CV1 represents the coordination number (CN) of the carbonyl oxygen O_3 to all water protons and CV2 the CN of the carbonyl carbon C_1 to all water oxygens with:[56,57]

$$CN = \sum_i \frac{1 - (d_i/d_0)^p}{1 - (d_i/d_0)^{p+q}} \tag{1}$$

where d_i is the distance between the O_3 and the i^{th} solvent hydrogen ($d_0 = 1.4$ Å) or between C_1 and the i^{th} solvent oxygen ($d_0 = 1.8$ Å), $p = 6$ and $q = 6$. Thus a CN value close to one corresponds to a coordinated atom while a CN value approaching zero means that the atom is free. We have checked a posteriori that this choice of CVs led to clearly separated basins for the reactant, product, and transition state. It is a minimum criterion to be fulfilled for an MTD simulation. In total, more than nine thousand hills were accumulated along the MTD trajectory, during which the forward transition from the keto form to the gem-diol was sampled twice and the reverse transition twice. The MTD simulation was stopped when the oxygen atom of the carbonyl group O_3 was detached from the carbon atom C_1, a few MD steps before the formation of the keto form, since the first CV could not be relevant anymore.

Excited states

The vertical excited states transition energies were computed using the TURBOMOLE package[58] with the algebraic diagrammatic construction through second-order, ADC(2),[59,60] with the RI scheme,[61] and the frozen core approximation. The def2-TZVPP extended atomic basis set was used. Based on a benchmark on 80 molecules, the ADC(2) had been recommended instead of TD-DFT, especially for keto dyes (with at least one carbonyl group), yielding results that are similar to the CC2 method for an acceptable computational effort.[62] Since a recent issue has been raised regarding the application of this method to molecules bearing a carbonyl group,[63] we carefully checked that the error on the vertical excited state energies of

K1, K2, and K3 configurations was less than 0.25 eV with respect to CC2 calculations (see Table S1 in Supplementary Information). To visualize the excitations, occupied and virtual natural transition orbitals (NTOs) were obtained from a singular value decomposition of the excitation amplitudes.[64]

Acknowledgements

This work was supported by the ANR DYNAAMIX project (ANR-17-CE29-0001-01) of the French Agence Nationale de la Recherche. This work was granted access to the HPC resources of CINES under the allocation 2020-A0100810750 made by GENCI (Grand Equipement National de Calcul Intensif).

Conflict of Interest

There are no conflicts to declare.

References

(1) Pöschl, U.; Shiraiwa, M. Multiphase Chemistry at the Atmosphere–Biosphere Interface Influencing Climate and Public Health in the Anthropocene. *Chem. Rev.* **2015**, *115*, 4440–4475.

(2) Chebbi, A.; Carlier, P. Carboxylic acids in the troposphere, occurrence, sources, and sinks: A review. *Atmos. Environ.* **1996**, *30*, 4233–4249.

(3) Agarwal, S.; Aggarwal, S. G.; Okuzawa, K.; Kawamura, K. Size distributions of dicarboxylic acids, ketoacids, α-dicarbonyls, sugars, WSOC, OC, EC and inorganic ions in atmospheric particles over Northern Japan: Implication for long-range transport of Siberian biomass burning and East Asian polluted aerosols. *Atmos. Chem. Phys.* **2010**, *10*, 5839–5858.

(4) Hoque, M. M. M.; Kawamura, K.; Nagayama, T.; Kunwar, B.; Peltzer, E. T.; Gagosian, R. B. Molecular characteristics of water-soluble dicarboxylic acids, -oxocarboxylic acids, pyruvic acid and -dicarbonyls in the aerosols from the eastern North Pacific. *Marine Chemistry* **2020**, *224*, 103812.

(5) Herrmann, H. Kinetics of aqueous phase reactions relevant for atmospheric chemistry. *Chem. Rev.* **2003**, *103*, 4691–4716.

(6) Cheng, Y.; Zheng, G.; Wei, C.; Mu, Q.; Zheng, B.; Wang, Z.; Gao, M.; Zhang, Q.; He, K.; Carmichael, G. et al. Reactive nitrogen chemistry in aerosol water as a source of sulfate during haze events in China. *Sci. Adv.* **2016**, *2*, 1–11.

(7) Herrmann, H.; Schaefer, T.; Tilgner, A.; Styler, S. A.; Weller, C.; Teich, M.; Otto, T. Tropospheric Aqueous-Phase Chemistry: Kinetics, Mechanisms, and Its Coupling to a Changing Gas Phase. *Chem. Rev.* **2015**, *115*, 4259–4334.

(8) Mekic, M.; Brigante, M.; Vione, D.; Gligorovski, S. Exploring the ionic strength effects on the photochemical degradation of pyruvic acid in atmospheric deliquescent aerosol particles. *Atmospheric Environment* **2018**, *185*, 237–242.

(9) Shedge, S. V.; Zuehlsdorff, T. J.; Servis, M. J.; Clark, A. E.; Isborn, C. M. Effect of Ions on the Optical Absorption Spectra of Aqueously Solvated Chromophores. *The Journal of Physical Chemistry A* **2019**, *123*, 6175–6184.

(10) Mkoma, S. L.; Kawamura, K. Molecular composition of dicarboxylic acids, ketocarboxylic acids, α-dicarbonyls and fatty acids in atmospheric aerosols from Tanzania, East Africa during wet and dry seasons. *Atmos. Chem. Phys.* **2013**, *13*, 2235–2251.

(11) Ervens, B. Modeling the Processing of Aerosol and Trace Gases in Clouds and Fogs. *Chem. Rev.* **2015**, *115*, 4157–4198.

(12) Xia, S.-S.; Eugene, A. J.; Guzman, M. I. Cross Photoreaction of Glyoxylic and Pyruvic Acids in Model Aqueous Aerosol. *J. Phys. Chem. A* **2018**, *122*, 6457–6466.

(13) Guzman, M. I.; Eugene, A. J. Aqueous Photochemistry of 2-Oxocarboxylic Acids: Evidence, Mechanisms, and Atmospheric Impact. *Molecules* **2021**, *26*, 5278.

(14) Rapf, R. J.; Dooley, M. R.; Kappes, K.; Perkins, R. J.; Vaida, V. pH Dependence of the Aqueous Photochemistry of α-Keto Acids. *The Journal of Physical Chemistry A* **2017**, *121*, 8368–8379.

(15) Shemesh, D.; Luo, M.; Grassian, V. H.; Gerber, R. B. Absorption spectra of pyruvic acid in water: insights from calculations for small hydrates and comparison to experiment. *Phys. Chem. Chem. Phys.* **2020**, *22*, 12658–12670.

(16) Luo, M.; Shemesh, D.; Sullivan, M. N.; Alves, M. R.; Song, M.; Gerber, R. B.; Grassian, V. H. Impact of pH and NaCl and CaCl2 Salts on the Speciation and Photochemistry of Pyruvic Acid in the Aqueous Phase. *The Journal of Physical Chemistry A* **2020**, *124*, 5071–5080.

(17) Eugene, A. J.; Guzman, M. I. Cross Photoreaction of Glyoxylic and Pyruvic Acids in Model Aqueous Aerosol. *The Journal of Physical Chemistry A* **2018**, *122*, 6457–6466.

(18) Lewis, J. S.; Gaunt, A. P.; Comment, A. Photochemistry of pyruvic acid is governed by photo-induced intermolecular electron transfer through hydrogen bonds. *Chem. Sci.* **2022**, *13*, 11849–11855.

(19) Guzmàn, M. I.; Colussi, A. J.; Hoffmann, M. R. Photoinduced Oligomerization of Aqueous Pyruvic Acid. *J. Phys. Chem. A* **2006**, *110*, 3619–3626.

(20) Grgić, I.; Nieto-Gligorovski, L. I.; Net, S.; Temime-Roussel, B.; Gligorovski, S.; Wortham, H. Light induced multiphase chemistry of gas-phase ozone on aqueous pyruvic and oxalic acids. *Phys. Chem. Chem. Phys.* **2010**, *12*, 698–707.

(21) Griffith, E. C.; Carpenter, B. K.; Shoemaker, R. K.; Vaida, V. Photochemistry of aqueous pyruvic acid. *The Proceedings of the National Academy of Sciences* **2013**, *110*, 11714–11719.

(22) Reed Harris, A. E.; Ervens, B.; Shoemaker, R. K.; Kroll, J. A.; Rapf, R. J.; Griffith, E. C.; Monod, A.; Vaida, V. Photochemical kinetics of pyruvic acid in aqueous solution. *J. Phys. Chem. A* **2014**, *118*, 8505–8516.

(23) Boris, A. J.; Desyaterik, Y.; Collett, J. L. How do components of real cloud water affect aqueous pyruvate oxidation? *Atmospheric Research* **2014**, *143*, 95–106.

(24) Eugene, A. J.; Guzman, M. I. Reactivity of Ketyl and Acetyl Radicals from Direct Solar Actinic Photolysis of Aqueous Pyruvic Acid. *The Journal of Physical Chemistry A* **2017**, *121*, 2924–2935.

(25) Eugene, A. J.; Guzman, M. I. Production of Singlet Oxygen (1O2) during the Photochemistry of Aqueous Pyruvic Acid: The Effects of pH and Photon Flux under Steady-State O2(aq) Concentration. *Environmental Science & Technology* **2019**, *53*, 12425–12432.

(26) Lopalco, A.; Douglas, J.; Denora, N.; Stella, V. J. Determination of pKa and Hydration Constants for a Series of α-Keto-Carboxylic Acids Using Nuclear Magnetic Resonance Spectrometry. *J. Pharm. Sci.* **2016**, *105*, 664–672.

(27) Pocker, Y.; Meany, J. E.; Nist, B. J.; Zadorojny, C. Reversible hydration of pyruvic acid. I. Equilibrium studies. *J. Phys. Chem.* **1969**, *73*, 2879–2882.

(28) Leermakers, P. A.; Vesley, G. F. Photolysis of Pyruvic Acid in Solution. *J. Org. Chem.* **1963**, *28*, 1160–1161.

(29) Leermakers, P. A.; Vesley, G. F. The Photochemistry of alpha-Keto Acids and alpha-Keto Esters. I. Photolysis of Pyruvic Acid and Benzoylformic Acid. *J. Am. Chem. Soc.* **1963**, *85*, 3776–3779.

(30) Blair, S. L.; Reed Harris, A. E.; Frandsen, B. N.; Kjaergaard, H. G.; Pangui, E.;

Cazaunau, M.; Doussin, J.-F.; Vaida, V. Conformer-Specific Photolysis of Pyruvic Acid and the Effect of Water. *The Journal of Physical Chemistry A* **2020**, *124*, 1240–1252.

(31) Fischer, M.; Warneck, P. The Dissociation Constant of Pyruvic Acid: Determination by Spectrophotometric Measurements. *Ber. Bunsen Phys. Chem.* **1991**, *95*, 523–527.

(32) Pollet, R.; Chin, W. Reversible Hydration of α-Dicarbonyl Compounds from Ab Initio Metadynamics Simulations: Comparison between Pyruvic and Glyoxylic Acids in Aqueous Solutions. *The Journal of Physical Chemistry B* **2021**, *125*, 2942–2951.

(33) Clarke, C.; Gibbard, J.; Hutton, L.; Verlet, J.; Curchod, B. Photochemistry of the pyruvate anion produces CO2, CO, CH3–, CH3, and a low energy electron. *Nature Communications* **2022**, *13*, 937.

(34) Lesnicki, D.; Wank, V.; Cyran, J. D.; Backus, E. H. G.; Sulpizi, M. Lower degree of dissociation of pyruvic acid at water surfaces than in bulk. *Phys. Chem. Chem. Phys.* **2022**, *24*, 13510–13513.

(35) Shedge, S. V.; Zuehlsdorff, T. J.; Servis, M. J.; Clark, A. E.; Isborn, C. M. Effect of Ions on the Optical Absorption Spectra of Aqueously Solvated chromophores. *The Journal of Physical Chemistry A* **2019**, *123*, 6175–6184.

(36) Loisel, G.; Mekic, M.; Liu, S.; Song, W.; Jiang, B.; Wang, Y.; Deng, H.; Gligorovski, S. Ionic strength effect on the formation of organonitrate compounds through photochemical degradation of vanillin in liquid water of aerosols. *Atmospheric Environment* **2021**, *246*, 118140.

(37) Barquilla, M. D. P.; Mayes, M. L. Role of hydrogen bonding in bulk aqueous phase decomposition, complexation, and covalent hydration of pyruvic acid. *Phys. Chem. Chem. Phys.* **2022**, *24*, 25151–25170.

(38) Cao, W.; Hu, Z.; Peng, X.; Sun, H.; Sun, Z.; Wang, X.-B. Annihilating Actinic Photochemistry of the Pyruvate Anion by One and Two Water Molecules. *Journal of the American Chemical Society* **2022**, *144*, 19317–19325.

(39) Yang, D.; Zhang, L. Excited-state hydrogen bonding dynamics of pyruvic acid and geminal-diol, 2,2-dihydroxypropanoic acid in aqueous solution: a DFT/TDDFT study. *J. Phys. Org. Chem.* **2012**, *25*, 1391–1394.

(40) Dommer, A. C.; Wauer, N. A.; Angle, K. J.; Davasam, A.; Rubio, P.; Luo, M.; Morris, C. K.; Prather, K. A.; Grassian, V. H.; Amaro, R. E. Revealing the Impacts of Chemical Complexity on Submicrometer Sea Spray Aerosol Morphology. *ACS Central Science* **2023**, *9*, 1088–1103.

(41) Gao, Z.-F.; Di, Y.-Y.; Liu, S.-Z.; Lu, D.-F.; Dou, J.-M. Crystal structure and thermochemical properties of a novel coordination compound sodium pyruvate C3H3O3Na(s). *The Journal of Chemical Thermodynamics* **2014**, *78*, 189–196.

(42) Eugene, A. J.; Xia, S.-S.; Guzman, M. I. Aqueous Photochemistry of Glyoxylic Acid. *The Journal of Physical Chemistry A* **2016**, *120*, 3817–3826.

(43) Hazra, M. K.; Francisco, J. S.; Sinha, A. Hydrolysis of Glyoxal in Water-Restricted Environments: Formation of Organic Aerosol Precursors through Formic Acid Catalysis. *The Journal of Physical Chemistry A* **2014**, *118*, 4095–4105.

(44) Axson, J. L.; Takahashi, K.; Haan, D. O. D.; Vaida, V. Gas-phase water-mediated equilibrium between methylglyoxal and its geminal diol. *Proceedings of the National Academy of Sciences* **2010**, *107*, 6687–6692.

(45) Bussi, G.; Laio, A. Using metadynamics to explore complex free-energy landscapes. *Nat. Rev. Phys.* **2020**, *2*, 200–212.

(46) Marx, D.; Hutter, J. *Ab initio Molecular Dynamics: Basic Theory and Advanced Methods*; Cambridge University Press: Cambridge, 2009.

(47) Car, R.; Parrinello, M. Unified Approach for Molecular Dynamics and Density-Functional Theory. *Phys. Rev. Lett.* **1985**, *55*, 2471–2474.

(48) Bussi, G.; Laio, A.; Tiwary, P. In *Handbook of Materials Modeling: Methods: Theory and Modeling*; Andreoni, W., Yip, S., Eds.; Springer International Publishing: Cham, 2020; pp 565–595.

(49) Bussi, G.; Branduardi, D. *Reviews in Computational Chemistry Volume 28*; John Wiley & Sons, Ltd, 2015; Chapter 1, pp 1–49.

(50) Laio, A.; Gervasio, F. L. Metadynamics: a method to simulate rare events and reconstruct the free energy in biophysics, chemistry and material science. *Rep. Prog. Phys.* **2008**, *71*, 126601.

(51) Ensing, B.; Laio, A.; Parrinello, M.; Klein, M. L. A Recipe for the Computation of the Free Energy Barrier and the Lowest Free Energy Path of Concerted Reactions. *J. Phys. Chem. B* **2005**, *109*, 6676–6687.

(52) Laio, A.; Parrinello, M. *Proc. Natl. Acad. Sci. USA* **2002**, *99*, 12562–12566.

(53) The CPMD program is © 1990-2023 by IBM Corp. and © 1994-2001 by Max Planck Institute, Stuttgart.

(54) Vanderbilt, D. Soft self-consistent pseudopotentials in a generalized eigenvalue formalism. *Phys. Rev. B* **1990**, *41*, 7892–7895.

(55) Jabraoui, H.; Charpentier, T.; Gin, S.; Delaye, J.-M.; Pollet, R. Behaviors of sodium and calcium ions at the borosilicate glass–water interface: Gaining new insights through an ab initio molecular dynamics study. *The Journal of Chemical Physics* **2022**, *156*, 134501.

(56) Stirling, A.; Iannuzzi, M.; Laio, A.; Parrinello, M. Azulene-to-Naphthalene Rearrangement: The Car–Parrinello Metadynamics Method Explores Various Reaction Mechanisms. *ChemPhysChem* **2004**, *5*, 1558–1568.

(57) Iannuzzi, M.; Laio, A.; Parrinello, M. Efficient Exploration of Reactive Potential Energy Surfaces Using Car-Parrinello Molecular Dynamics. *Phys. Rev. Lett.* **2003**, *90*, 238302.

(58) TURBOMOLE V7.3 2018, a development of University of Karlsruhe and Forschungszentrum Karlsruhe GmbH, 1989-2007, TURBOMOLE GmbH, since 2007; available from
`http://www.turbomole.com`.

(59) Schirmer, J. Beyond the random-phase approximation: A new approximation scheme for the polarization propagator. *Phys. Rev. A* **1982**, *26*, 2395–2416.

(60) Trofimov, A. B.; Schirmer, J. An efficient polarization propagator approach to valence electron excitation spectra. *Journal of Physics B: Atomic, Molecular and Optical Physics* **1995**, *28*, 2299–2324.

(61) Hättig, C. In *Response Theory and Molecular Properties (A Tribute to Jan Linderberg and Poul Jørgensen)*; Jensen, H., Ed.; Advances in Quantum Chemistry; Academic Press, 2005; Vol. 50; pp 37–60.

(62) Jacquemin, D.; Duchemin, I.; Blase, X. 0–0 Energies Using Hybrid Schemes: Benchmarks of TD-DFT, CIS(D), ADC(2), CC2, and BSE/GW formalisms for 80 Real-Life Compounds. *Journal of Chemical Theory and Computation* **2015**, *11*, 5340–5359.

(63) Marsili, E.; Prlj, A.; Curchod, B. F. E. Caveat when using ADC(2) for studying the photochemistry of carbonyl-containing molecules. *Phys. Chem. Chem. Phys.* **2021**, *23*, 12945–12949.

(64) Martin, R. L. Natural transition orbitals. *The Journal of Chemical Physics* **2003**, *118*, 4775–4777.